The Journal of Chemical Physics

RESEARCH ARTICLE | MAY 15 2023

Functionalized carbon nanocones performance in water harvesting

Special Collection: Chemical Physics of Controlled Wettability and Super Surfaces

Fernanda R.Leivas ✉ ; Marcia C. Barbosa

J. Chem. Phys. 158, 194702 (2023)
https://doi.org/10.1063/5.0142718

The Journal of Chemical Physics ARTICLE scitation.org/journal/jcp

Functionalized carbon nanocones performance in water harvesting

Cite as: J. Chem. Phys. 158, 194702 (2023); doi: 10.1063/5.0142718
Submitted: 16 January 2023 • Accepted: 30 April 2023 •
Published Online: 15 May 2023

Fernanda R. Leivas[a] and Marcia C. Barbosa[b]

AFFILIATIONS

Instituto de Física, Universidade Federal do Rio Grande do Sul, CP 15051, 91501-970 Porto Alegre, RS, Brazil

Note: This paper is part of the JCP Special Topic on Chemical Physics of Controlled Wettability and Super Surfaces.
[a]**Author to whom correspondence should be addressed:** fernanda.leivas@ufrgs.br
[b]**Electronic mail:** marcia.barbosa@ufrgs.br

ABSTRACT

In this work, we investigate the water capture process for functionalized carbon nanocones (CNCs) through molecular dynamic simulations in the following three scenarios: a single CNC in contact with a reservoir containing liquid water, a single CNC in contact with a water vapor reservoir, and a combination of more than one CNC in contact with vapor. We found that water flows through the nanocones when in contact with the liquid reservoir if the nanocone tip presents hydrophilic functionalization. In contact with steam, we observed the formation of droplets at the base of the nanocone only when hydrophilic functionalization is present. Then, water flows through in a linear manner, a process that is more efficient than that in the liquid reservoir regime. The scalability of the process is tested by analyzing the water flow through more than one nanocone. The results suggest that the distance between the nanocones is a fundamental ingredient for the efficiency of water harvesting.

I. INTRODUCTION

Water, composing up to 60% of the human body, is fundamental in many biochemical processes.[1] Despite covering about 70% of the Earth's surface, potable water scarcity is one of the biggest global challenges of today.[2,3] With climate changes, even countries with abundant drinking water, like Brazil, are suffering with water scarcity.[4] The impact of a drought is not just restricted to rural areas but also affects the labor market of metropolitan regions.[5,6]

Water is a basic necessity for human survival. Finding alternatives to circumvent the problem of water shortage can prevent an imminent catastrophe. Among the alternatives available today, air is a possible source of freshwater water. Fog is composed of micrometer water droplets created when the air becomes saturated with water vapor. At this size, the droplets float on air, and they can deposit on surfaces due to water-water and water-surface interactions. Since it is accessible everywhere, new modern and sustainable methods for fog harvesting are being developed.[7–12]

One of the effects of global warming is the increase in humidity in the atmosphere, causing an increase in the average temperature of the Earth's surface.[13] Thus, developing an efficient atmospheric water harvesting (AWH) method to remove excess moisture can help combat climate change.

The main problem with the existing commercial atmospheric water generators is that they are generally energetically expensive.[14] The process of collecting water from the air has two requirements: the presence of high humidity with the ability to wet a surface and a process for gathering the droplets. If the available air is not humid enough, water generators cool the air ambient below its dew point (dew water harvesting), which represents an additional energy cost for the process.[7] In the presence of humidity, the challenge is to move the droplets and collect them into a reservoir. One strategy is the biomimic designs that use capillarity, Laplace pressure, and hydrophobicity[15–18] to move water. These strategies use classical hydrodynamics and gravity as driving forces.

Water has more than 70 thermodynamic, dynamic, and structural anomalies both on bulk[1] and on confined water.[19,20] For instance, at the nanoscale, water violates the classical hydrodynamics.[21,22] Under confinement in carbon nanotubes (CNT), it flows under pressure faster than what the classical hydrodynamics predicts.[23] These phenomena happen due to the increase

of the slip length activated by the single line move of the water molecules[21,22] inside the nanotubes with a diameter smaller than 2 nm.

The fast mobility of water inside carbon nanotubes can be used to create a more efficient process of separating water from salt[24–26] or also can be used on selective filters.[27–29] Due to the good flow rate of confined water, it becomes natural to think of combining the surface wetting in a humid environment with the high mobility of nanoconfined water to produce an efficient atmospheric water harvesting process. The challenge is how to make the water enter the confined structure without the use of a huge pressure gradient.

The use of hydrophilic functionalization to promote water entrance in nanotubes is not new.[30,31] Sorption-based AWH devices, derived from carbon nanoporous functionalized, are presenting a high performance in water collection.[32–35] In all these cases, the use of pressure is still present. In addition to the nanotubes, carbon nanocones (CNCs) also present high efficiency in water transport.[36] Previous works have been also demonstrated the potential of this nanometric canonical structure.[27,37] The nanocones when functionalized with charges[38] or under an external field[39] show a good performance in desalination.[28] Recently, we proposed an atmospheric water harvesting process using a carbon nanocone functionalized with a hydrophilic material.[40] We found that this functionalized nanocone is able to capture water from vapor in a rapid and continuous flow without the use of pressure.[40]

The conical geometry of nanopores is highly advantageous as it functions like a funnel, facilitating the entrance of molecules into the nanopore. The synthesis of carbon nanocones is not complicated,[41,42] and they are already being commercialized by Carbonium SRL. Furthermore, various reduction techniques, void nanocones, and types of functionalization have been reported.[43–45]

The water flow through polymeric membranes usually depends on the size, shape, and length of the individual pores,[46,47] as well as on the density of pores.[48] However, at the nanoscale, the impact of the density of pores is still not clear. Although for the water flow through MoS_2 nanopores, the distance between the pores does not show a significant hydrodynamic interaction[49] for double nano-interlayer membranes, and the surface porosity impacts the nanofiltration performance.[50] The distinction between these two systems is the hydrophobicity and the geometry. Consequently, how the distribution of combined nanocones affects water capture dynamics is still an open question.

In this work, we investigate the process of capturing water by a functionalized carbon nanocone using molecular dynamics simulations. We analyze how the distribution of nanocones affects water vapor harvesting. We also compare the capturing and flow of water by the nanocone in two distinct scenarios: the nanocone in contact with a liquid water reservoir and in contact with a vapor reservoir.

The remainder of this paper goes as follows: In Sec. II, the model is described in the different scenarios analyzed, and the simulation details are presented. Section III shows the results, and conclusions are discussed in Sec. IV.

II. MODEL

We study three systems: a single nanocone in contact with a liquid water reservoir, a single nanocone in contact with a vapor reservoir, and a combination of nanocones in contact with a vapor reservoir.

The systems with single nanocones are illustrated in Fig. 1. They are composed of a conical carbon nanochannel coupled to two slabs: a carbon slab at the nanocone base and a hydrophilic slab at the nanocone tip. Both slabs have a size L^2 Å^2, with $L = 50$ Å.

The carbon slab is made of carbon atoms (gray) and the hydrophilic slab is made of hydrophilic particles (green). All the slabs are maintained rigid during the simulation. The carbon slab is in contact with a reservoir, which contains water in the liquid phase, shown in Fig. 1(a), or in the vapor phases, illustrated in Fig. 1(b). The hydrophilic slab, present in both cases, is in contact with a vacuum reservoir.

Systems with multiple nanocones have been analyzed for $L = 60, 80$Å.

A. Liquid reservoir

The left side of the system shown in Fig. 1(a) has a water reservoir of size $50 \times 20 \times 50$ Å^3, and temperature is kept constant at 300 K. This reservoir is in contact with the carbon slab of 50×50 Å^2 and a nanocone with dimensions defined below.

The number of water molecules used in this simulation is 1763 with a density of 0.96 g/cm^3. Initially, the resulting pressure of the water confined in the liquid reservoir is about 61 MPa. To calculate the pressure in the liquid reservoir region, we used the per-atom stress, since it is the negative of the per-atom pressure tensor. Hence, the total pressure is the diagonal component of the per-atom stress divided by the volume and dimension of system $(3V)$,

$$P = \frac{ps_x + ps_y + ps_z}{3V}. \quad (1)$$

In Eq. (1), ps_x, ps_y, and ps_z are the result of the per-atom stress tensor summed for all atoms. These components were calculated using the compute stress/atom command in LAMMPs.

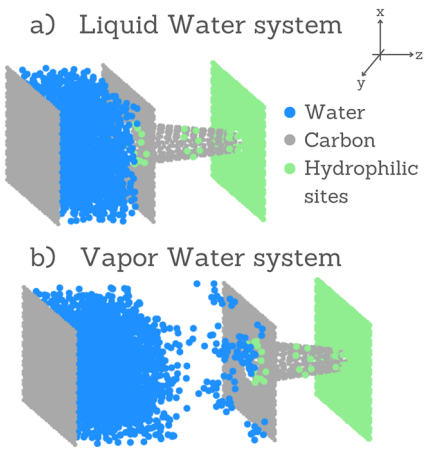

FIG. 1. A snapshot of the simulation system. (a) Liquid water and (b) vapor reservoir in contact with a carbon slab and with the nanocone hydrophilic base. The nanocone tip is in contact with the hydrophilic slab at a collecting reservoir.

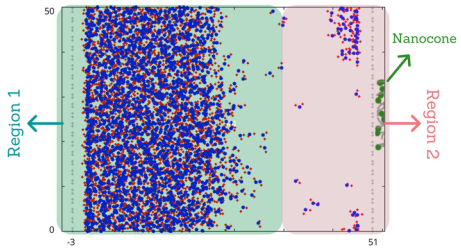

FIG. 2. Part of the simulation box illustrating the two types of thermal control used in the simulation. The blue turquoise region represents thermostat 1, with the temperature dynamically changing between 800 and 300 K and thermostat 2 with the temperature fixed at 300 K.

B. Vapor reservoir

To produce vapor, we employ the following strategy. The left side of the system shown in Fig. 1(b) has a water reservoir of dimensions $50 \times 54 \times 50$ Å^3.

Initially, the number of water molecules on this reservoir is 1473, with a density of 0.38 g/cm^3, which corresponds a vapor–liquid region for the 300 K.[51] To separate the liquid and vapor phases, we use two thermostats with different temperatures, as illustrated in Fig. 2. Region 1 contains water in the liquid phase, and region 2, in the vapor phase. The vapor in region 2 is produced from the liquid phase in the blue region. To produce vapor, a dynamical process of temperature variation, from 800 to 300 K every 10 000 temporal steps, was implemented in region 1. Region 2 maintains the temperature constant at 300 K during all simulations, and it is in contact with the carbon slab of 50×50 Å^2 size and nanocone entrance with dimensions defined below.

The idea of using combined thermostats to produce vapor has already been employed in other works to reproduce water evaporation and condensation.[40,52,53]

The temporal evolution of density and temperature for a chunk $z = [0.30, 0.38]$ Å at region 2 (vapor region) is shown in Figs. 3(a) and 3(b). The density has a mean value of 0.23 ± 0.09 g/cm^3, whereas the temperature has a mean value of 270 ± 109.9 K. These values correspond to the vapor phase on the TIP4P phase diagram.[54] As our system is not in equilibrium, the temperature fluctuates significantly due to the energetic particles coming from region 1 that disturb the equilibrium in region 2. Additionally, the chunk being analyzed has a very small density, resulting in low statistics. However, the mean temperature of 270 K is close to the thermostat temperature of region 2 (300 K). The TIP4P/2005 model used in our simulation provides a satisfactory description of self-diffusion coefficient,[55] phase diagram, vapor–liquid equilibrium,[56,57] vapor pressure, and critical temperature. Therefore, the gas produced in our simulations replicates the basic properties expected from the vapor phase.

C. Water collector reservoir

The right side of the systems consists of a hydrophilic surface, which has the same atomic structure as the graphene slab. This surface limits the collector reservoir, which does not have water at the beginning of the simulation. The dimensions depend on the size of the hydrophilic slab in x and y directions and $z = 20$ Å. The

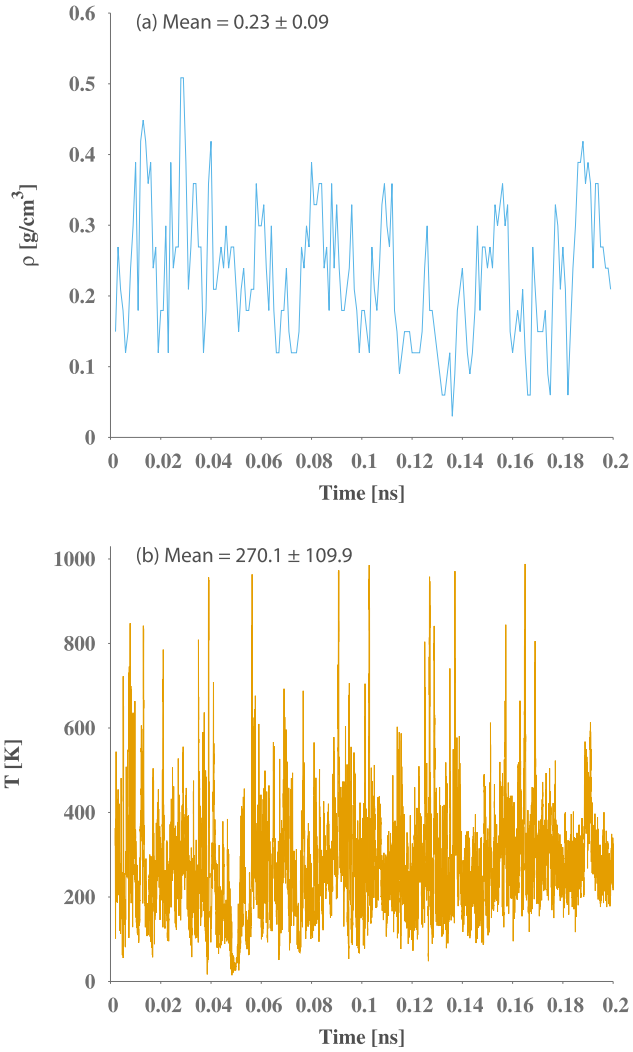

FIG. 3. (a) Temporal evolution of the density in the vapor region $z = [0.30, 0.38]$ Å. (b) Temporal evolution of the temperature in the vapor region.

water molecules collected by this reservoir are maintained under a thermostat with a temperature of 300 K, same as in region 2 (Fig. 2).

D. Nanocone

Between the liquid or vapor and the collector reservoirs, there is a conic carbon nanochannel with access to both sides as illustrated in Fig. 4. It has a length of 26 Å, and the base or the larger pore has a diameter of 17 Å, whereas the tip or the smaller pore has a diameter of 8.2 Å. The CNC is modeled with three hydrophilic regions: at the base, at the middle, and at the tip. The interactions between the atoms and water in these ring-shaped hydrophilic regions were calculated using an effective water wall potential ε_r. The CNC, as well as the carbon and hydrophilic slabs, remained fixed throughout the simulation. The water molecules inside the nanocone are subjected to a constant temperature thermostat of 300 K. The apex angle of the

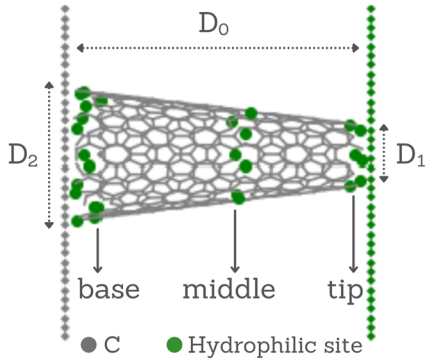

FIG. 4. Carbon nanocone with $D_0 = 26$ Å of length, $D_1 = 8.2$ Å of diameter of the base, and $D_2 = 17$ Å of diameter at the base. Hydrophilic rings are present at the base, tip, and middle of the nanocone.

nanocone used on simulations is 19.2°, despite it could be produced in five different apex angles.[58] We choose this angle because it is easier to produce in large scale[44] and is the nanocone, which achieves the higher values of water flux when compared with the others apex angles. It also presents a lower energy barrier when compared with carbon nanotubes (CNT).[36]

E. Combined nanocones

We also simulated two and four nanocones combined. In both cases, we divided the carbon slab into four squares. Two nanocones are symmetrically arranged at the center of the squares at opposite diagonals as illustrated in Fig. 5(a) with the distance between the nanocones $dr(L) = 34, 48$ with $L = 60, 80$ Å. Figure 5(b) shows four nanocones that are arranged in the center of each of the four parts with a distance between the nanocones of $dr(L)$ with $L = 60$ Å. In both systems, the vapor reservoir has dimensions $L \times 54 \times L$ Å^3.

The bases of the nanocones are coupled to a vapor reservoir as described in Subsection II B, but with variable dimensions, although the density is kept constant (0.38 g/cm^3). The number of molecules also varies with the dimensions of the system.

F. Simulation details

Simulation was conducted in the NVT ensemble with Molecular Dynamics (LAMMPs) using the TIP4P/2005[59] water model and Lennard-Jones (LJ) potential for the water–carbon interaction. The particle–particle mesh method, which solves the long-range interaction by Poisson's equation, was applied with a large cutoff of 13 Å to prevent errors associated with dispersion forces. The water model was chosen due to its good description of the water[55–57] and simplicity.[60,61] To keep the rigidity of water molecules, the SHAKE algorithm was employed.

The water–carbon Lennard-Jones (LJ) interaction was calculated using the Lorentz-Berthelot mixing rules,[62] resulting in $\varepsilon_{o-c} = 0.126$ kcal/mol and $\sigma_{o-c} = 3.279$ Å. The interaction between hydrophilic sites and water uses the same σ of carbon–oxygen interaction ($\sigma_{o-hs} = \sigma_{o-c}$), but the potential well was changed to $\varepsilon_{o-hs} = 1.1$ kcal/mol. This value was chosen because previous studies exploring different attractions show that this potential well optimizes the flow.[40] Modeling the functionalization as a Lennard-Jones interaction is an approximation since charge distribution of the functional groups is not taken into account. We do not expect this to change the behavior drastically.[63] The long-range electrostatic interaction was treated by the Particle–Particle Mesh Method, and the LJ cutoff distance was 12 Å. The force field and the atomistic model used in our simulations have been used in important works on water transport in nanomaterials.[29,38,39,64]

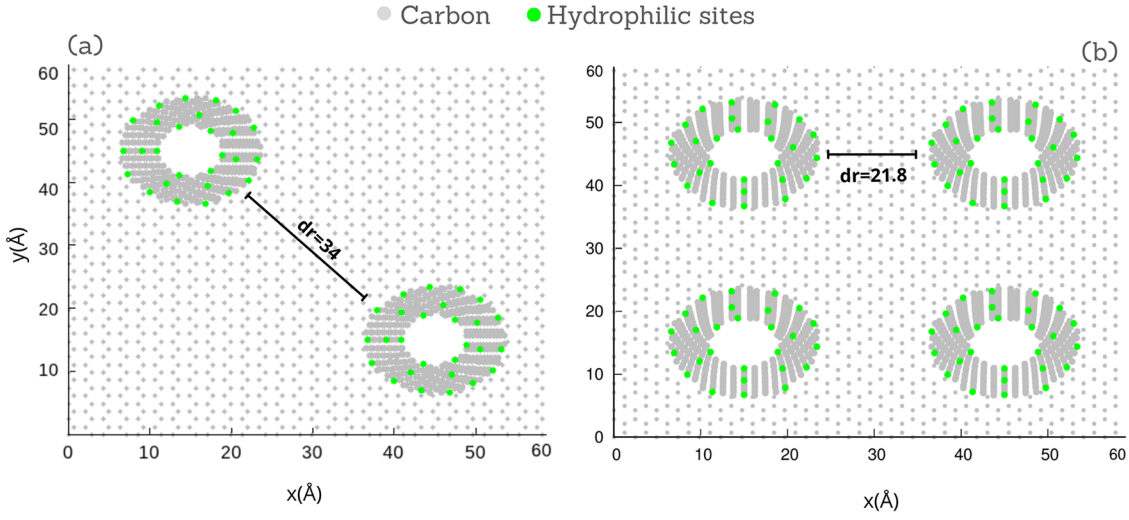

FIG. 5. System snapshot of the slab with (a) two and (b) four nanocones separated by distances $dr = 34$ and $dr = 21.8$, respectively, for $L = 60$ Å.

Periodic boundary conditions were applied in the x and y directions, and non-periodic boundary conditions were applied in the z direction (see Fig. 1).

III. RESULTS

We analyzed the water transport through nanocones in three scenarios: one hydrophilic nanocone base in contact with a liquid water reservoir, in contact with a water vapor reservoir, and combined nanocones in contact with a vapor water reservoir. The comparison between these scenarios is useful to identify the potential for capturing water of the harvesting process.

A. Liquid reservoir system

For a water molecule to enter into a nanostructure, it has to overcome electrostatic forces induced by the dielectric discontinuity between the water reservoir and the interface.[65] Usually, this is done by the use of external pressure[25,34] or electric field.[66] Here, we test a different strategy employing hydrophilic interactions as a driving force to move water molecules through the nanocone.

Figure 1(a) illustrates the first system we analyzed. It was composed by a liquid–water reservoir in contact with the base of the nanocone. We computed the number of water molecules that passed from the base to the tip (Fig. 4) and ends at the collector reservoir per time.

In the case of a completely hydrophobic nanocone (with no hydrophilic ring), some water molecules enter in the nanocone. The imbalance of chemical potential between the reservoir and the inner side of the nanocone induced a pressure gap of 61 MPa, which was enough to overcome the dielectric discontinuity at the nanocone entrance and make the water to enter. However, there is no water flow to the collector reservoir, since water molecules entered, but they did no leave the nanocone.

Therefore, for the water to pass through the nanocone, it needs to have at least a hydrophilic slab at the tip side. Hence, to understand the role of the hydrophilic structures in the water transport, we compared the amount of water obtained at the collector reservoir using two types of nanocones: one hydrophobic (but with a hydrophilic tip) and another with hydrophilic rings as illustrated in Fig. 4.

Figures 6(a) and 6(c) show the total number of molecules collected vs time for a nanocone with hydrophilic rings and a hydrophobic nanocone with the hydrophilic tip, respectively. We observe that the mobility of water molecules in both cases combines periods of increase in the number of water molecules collected with periods with no particle collected. The specific distribution of these two behaviors changes from sample to sample, but the presence of these two dynamics is observed in all.

Figures 6(b) and 6(d) show the histograms of the number of captured water molecules for different time intervals for the nanocone with hydrophilic rings and the hydrophobic rings, respectively. In both cases, there are time intervals in which water is collected followed by other time intervals with little or no molecules collected. The dynamics in the presence or absence of the hydrophilic rings are similar, in general, although the number of water molecules collected per unit of time is higher in the presence of hydrophilic rings.

Figures 6(a.1) and 6(c.1) show the mean and standard deviation calculated between three samples for each case. From these

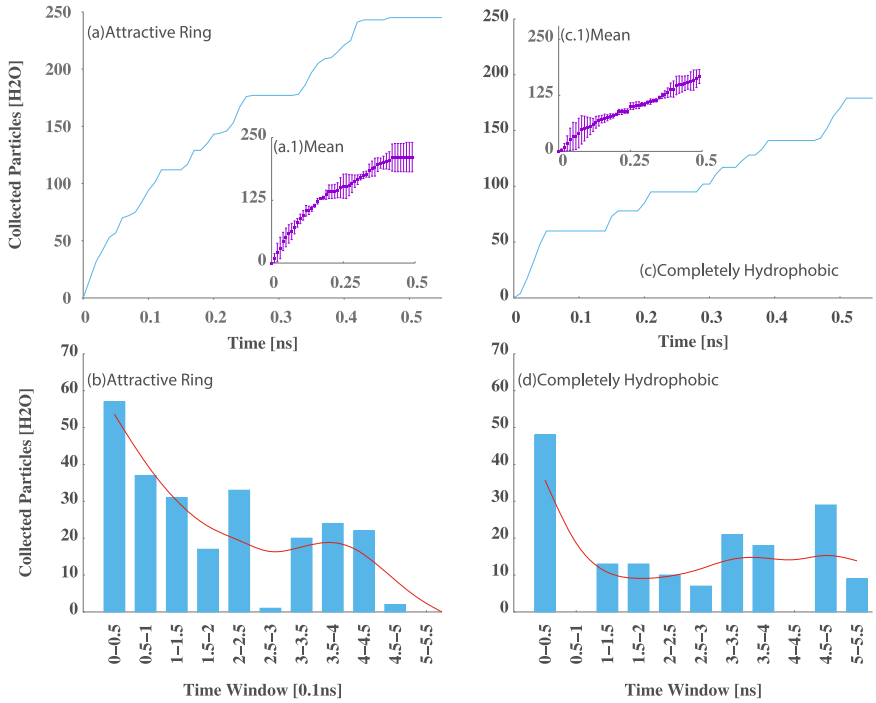

FIG. 6. The number of collected molecules vs time for a system (a) with hydrophilic rings and (C) without hydrophilic rings, and the mean (a.1) and (c.1) between five samples for each case. The histogram of the number of water molecules captured in different time intervals for the system with (b) hydrophilic rings and (d) without hydrophilic rings. The time starts when the first water molecule passes through the tip ring. The interaction with the hydrophilic wall is given by the attractive parameter $\varepsilon_r = 1.1$ kcal/mol.

data, we obtain the rate of captured molecules per 0.01 ns, the rate obtained from Fig. 6(a.1) was 4 ± 2.3 molecules/0.01 ns, whereas that from Fig. 6(c.1) was 2.91 ± 2.45 molecules/0.01 ns. These results suggest that the presence of the ring in the entrance and middle of the nanocone rings enhances the flow of water. Although in both cases, the entrance of water at the nanocone base is due to the water pressure from the liquid–water reservoir. The combination of the presence of hydrophilic sites, the asymmetric shape of the nanocone, and the presence of the hydrophilic slab in the tip of the nanocone creates a "flow direction." The additional rings in the three-ring system increases the mobility of water inside the nanocone.

Another strategy for moving water through a purely hydrophobic nanocone was presented by Li *et al.*[38] In their analysis, they employed an external pressure (100 MPa) to move water through a nanocone connecting two water reservoirs with the same density. Within their approach, they were able to transport 2 molecules/0.01 ns.

Our results suggests that the use of hydrophilic rings enhances water mobility. The drawback of our approach is that as particles move from the liquid reservoir to the collecting reservoir, the forces are balanced. The water collection stops when the pressure generated by the unbalanced chemical potential becomes too weak to induce the flow; hence, we observe the plateau at the end of Figs. 6(a) and 6(c).

B. Vapor reservoir system

Figure 1(b) illustrates the second system we analyzed: the nanocone in contact with a vapor reservoir. In a previous study, we showed that the vapor condenses at the carbon slab and the hydrophilic base of the nanocone, forming droplets,[40] which move inside the nanocone and are then captured at the collector reservoir. The impact of different attractions was also explored. Change the attraction on real life means change functionalization. We found that the potential well ε = 1.1 kcal/mol optimizes the flow, it is attractive enough to generate a high flux without trapping water molecules on the rings.

Succinctly, in the former study,[40] we showed that the dynamics of water transport goes as follows: First, there is a small droplets wetting time (SDWT), a period of 0.08 ns in which small droplets are condensed at the carbon slab and the nanocone base, attracted by the base hydrophilic ring, but they stay at the nanocone entrance. In this case, once the droplet is formed, it stays connected to the nanocone entrance because the water distribution is not large enough to be attracted by the hydrophilic ring in the middle of the nanocone.

Then follows a single droplets crossing time (SDCT), a period of time from [0 to 0.1] ns when the droplet at the nanocone base grows, some molecules are attracted to the central hydrophilic ring, and the droplet moves to the center and then to the nanocone tip leaving to the hydrophilic slab.

Next, there is a flowing time (FT), a period of time from [0.1 to 0.4] ns in which the carbon slab completely wets; at the nanocone base, a huge droplet is formed, creating a continuous flow driven by the hydrophilic strips along the nanocone. Finally, after 0.4 ns, the flow stops because the collector reservoir becomes full of water. Snapshots of the system illustrating these steps are present in Fig. 7.

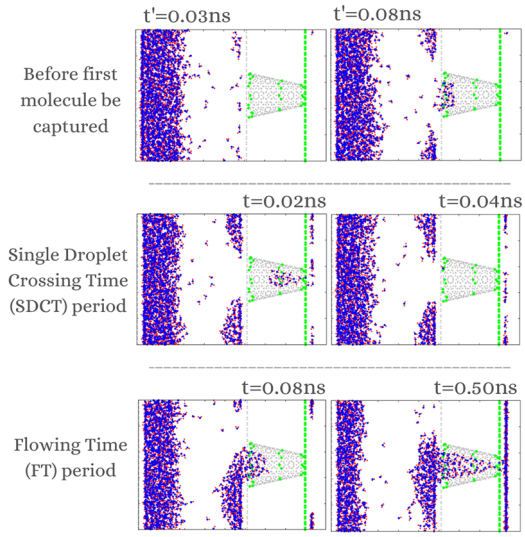

FIG. 7. Snapshots of the temporal evolution for vapor system using ε_i = 1.1 kcal/mol, showing the single droplet crossing (SDCT) time and the flowing time (FT).

Figure 8(a) displays the number of molecules collected by time for a single sample. The time intervals in this graph start when the first water molecule crosses the nanocone tip to the collector reservoir and, therefore, do not include the SDWT. On comparing Fig. 8(a) with Fig. 6(a), we can observe differences in water dynamics when changing the reservoir from liquid to vapor. It is noteworthy that in contrast to the chemical potential imbalance seen in the liquid reservoir case, the harvesting and collection of water in the vapor reservoir rely on the hydrophilic sites located on the nanocone. Figure 8(b) exhibits the mean and standard deviations of five samples for the FT regime. The rate of captured molecules per time is 9.91 ± 2.05 molecules/0.01 ns. Since we consider SDCT and SDWT as transition regimes and FT as a stationary regime, we have neglected the former two. The capture of molecules is limited by the size of the collector reservoir; if it were infinity, the system would continue to operate in the FT regime without saturating.

An important difference in the flow mechanism between the liquid and vapor reservoir systems is that in the former case, the flow

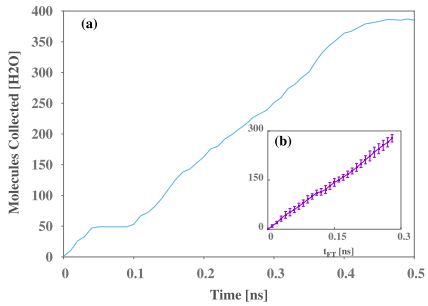

FIG. 8. (a) The number of collected water molecules vs time, and (b) the mean between five samples of the flowing time (FT) interval.

ceases when the collector reservoir is not full, whereas in the latter case, the flow stops only when the collector reservoir is full of particles. This distinct mechanism results in a linear flow rate of about 9.91 ± 2.05 molecules/0.01 ns for the vapor reservoir, which is higher than the non-linear flow rate of 4 ± 2.3 molecules/0.01 ns observed in the liquid reservoir.

C. Combined nanocones

Our results indicate that the system with a vapor reservoir is able to capture and collect water due to the presence of hydrophilic regions at the nanocone. Since mechanism behind this process depends on the wetting layer formed at the carbon slab, we can expect that the presence of multiple nanocones at the carbon slab might generate some competition, which affects the dynamics described in Subsection III B.

To test this assumption, we analyzed the systems with multiple nanocones, as illustrated in Fig. 5. We analyzed the system with two nanocones for L = 60 Å and L = 80 Å, whereas the system with four nanocones was studied for L = 60 Å.

Figure 9 illustrates the two-nanocones system, showing the number of water molecules captured by each nanocone (n1 and n2) for L = 60 Å and 80 Å using different initial conditions (C1 and C2). Figure 9(a) presents the system with L = 60 Å and dr = 34 Å for initial condition C1. For this distance, at the beginning 0.1 ns < t < 0.17 ns, the nanocone n1 enters in SDCT. For (t > 0.17 ns), the SDCT regime ends for the n1 nanocone, and for (t > 0.23 ns), n2 enters the FT regime. The same process happens for the initial condition C2, as shown in Fig. 9(b), but the transition occurs for (t > 0.28 ns). Figure 9(c) shows the mean and the standard deviation of the number of captured molecules in (0.01 ns) for each nanocones (n1 and n2), for C1 (green) and C2 (blue). In both cases, nanocone n1 has a low rate of captured particles compared with n2, indicating competition between them. Figures 9(d) and 9(e) also illustrate the capture mechanism but for a higher L = 80 Å. As L increases, the distance between nanocones dr also increases; hence, the competition

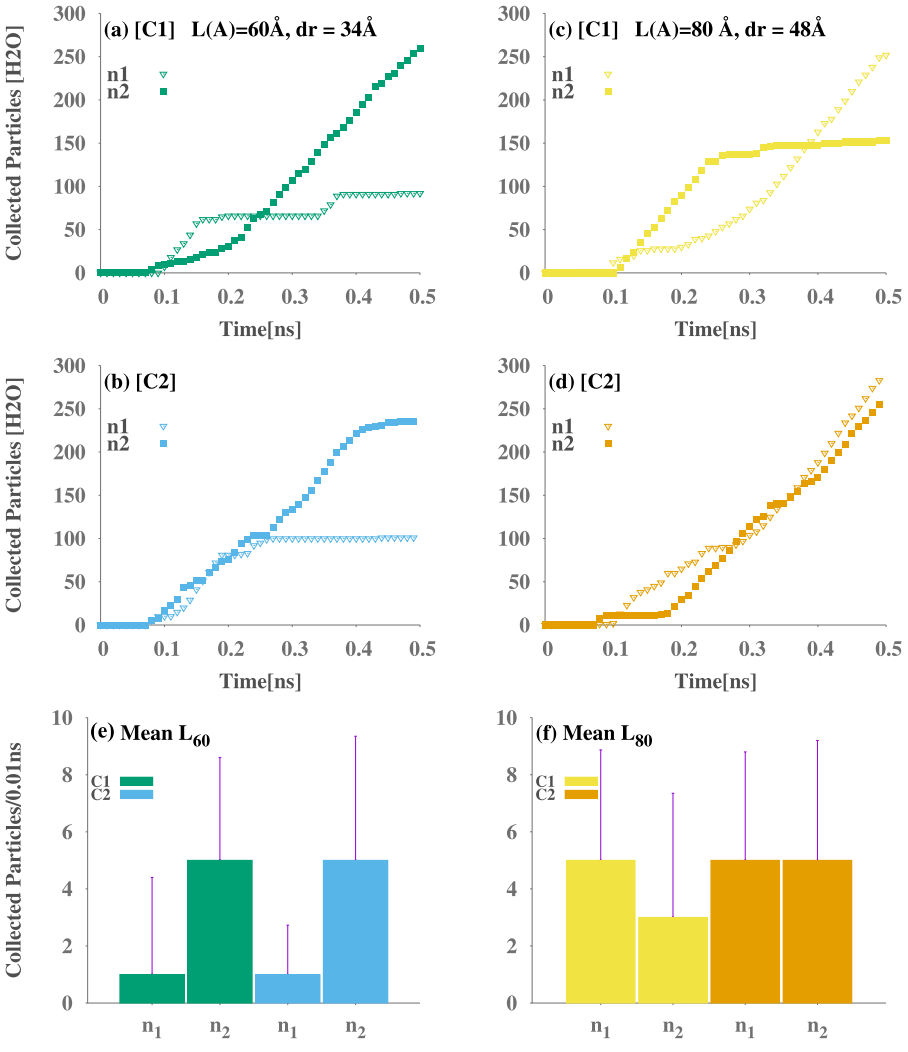

FIG. 9. Water molecules captured in time (ns) for systems with two nanocones (n1 and n2) for L = 60 Å with different initial conditions (a) C1 and (b) C2. For L = 80 Å also with different initial conditions (c) C1 and (d) C2. (e) and (f) show the mean and standard deviations of the number of molecules captured per 0.01 ns by each nanocone for L = 60 Å and L = 80 Å, respectively.

decreases. Figure 9(f) shows the mean and standard deviation of the rate of collected particles by time for $L = 80$ Å, where the collected rate difference between nanocones (competition) is lower (yellow-C1) or even nonexistent (orange-C2), when compared with $L = 60$ Å [Fig. 9(c)].

These results indicate that if the system does not have free surfaces for capturing water large enough, just one nanocone exhibits the FT regime. Note that regardless of the distance, the nanocones that reach the FT regime in Figs. 9(c) and 9(f) can be identified by the collected molecules rate of 6 molecules/0.01 ns, which is smaller than the rate found in a single nanocone in Sec. III B because here, the average is made for the entire simulation period and not just in a linear regime.

However, what happens if we increase the number of nanocones for the same reservoir dimensions? Does the competition remain the same or does the dynamic become more complex? In Fig. 10, we present the number of molecules collected vs time for each of the four nanocones, considering different initial conditions (c) C1 and (c) C2. Additionally, Figs. 10(b) and 10(d) show the mean and standard deviations of collected particles per 0.01 ns for each sample.

The size of the reservoir slab used was fixed at $L = 60$ Å, and the distance between the nanocones was $dr = 21.8$ Å. Based on Figs. 10(a) and 10(c), it can be observed that for all samples, the nanocones oscillate between absorption and non-absorption periods without any clear correlation between them. This behavior corresponds to the SDCT period, which results in a low collected rate for all nanocones, as seen in Figs. 10(b) and 10(d).

By increasing the number of nanocones, we decreased the effective space of the condensing area (carbon slab) at the same time that we increase the capture area (nanocone entrance). With this arrangement, there is no physical or temporal space for a large enough droplet to emerge in one of the nanocones base; hence, there is no linear regime. The vapor that arrives on the slab is quickly absorbed by one of the nanocones, resulting in alternating periods of absorption/non-absorption by the nanochannels without correlation. As a result, the nanocones remains in the SDCT regime without reaching the FT regime.

IV. CONCLUSIONS

We investigated water harvesting using a combination of hydrophobic and hydrophilic sites on a nanocone. First, we demonstrated that water can enter a hydrophobic nanocone, but it only flows through if the hydrophilic sites are present at the tip. This is a significant result as the water is expected to flow from a higher to a lower Laplace area, i.e., from the tip to the base of the nanocone. By carefully selecting the hydrophilicity/phobicity combination, we can obtain a contrary-to-Laplace gradient without using external pressure.

Then, we analyzed the water flow through the nanocone when it is in contact with the liquid–water reservoir. In this case, we observed a dynamic that depends on a chemical potential gradient combined with the hydrophilic sites. In this case, we observed that the flow water rate was 4 ± 2.3 molecules/0.01 ns.

Next, we observed how the water flows when the nanocone is in contact with the vapor reservoir. In this case, the water only enters the nanocone if hydrophilic sites would be present in the base and the tip of the nanocone. The dynamics is governed by the formation of droplets outside the nanocone. The cohesive forces present due to the asymmetric interactions with the hydrophilic sites promote a directional water movement. This leads to a linear regime, which is useful for moisture harvesting, with a flow rate of 9.91 ± 2.05 molecules/0.01 ns. The flow stops once the collecting

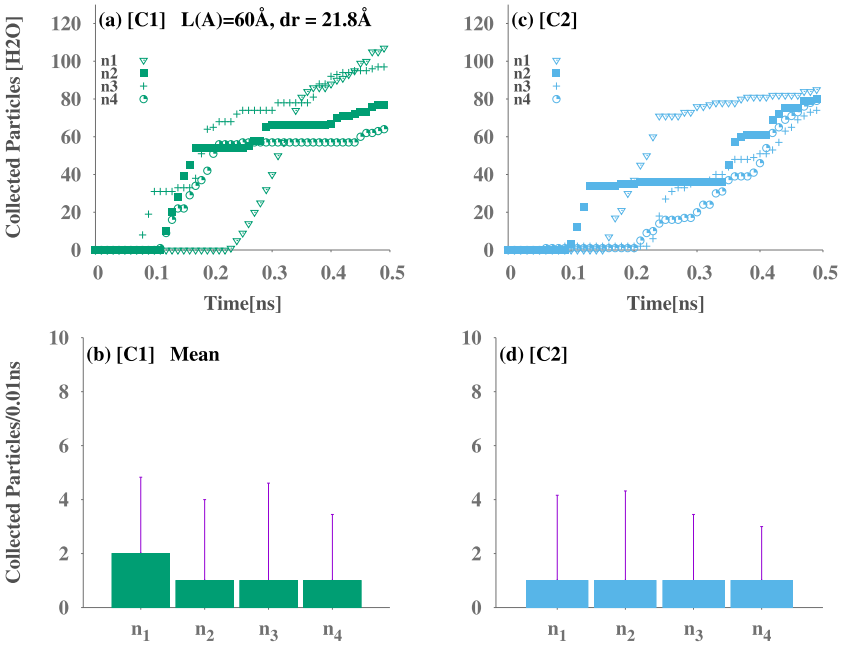

FIG. 10. Water molecules captured in time (ns) for systems with four nanocones (n1, n2, n3, and n4) for $L = 60$ Å with different initial conditions (a) C1 and (c) C2. (b) and (d) show the mean and standard deviations of the number of molecules captured per 0.01 ns by each nanocone for C1 and C2, respectively.

slab becomes full. Our results indicate that the capture mechanisms for liquid and vapor systems are distinct. The motion on the liquid reservoir depends on a chemical potential imbalance, whereas for the vapor reservoir, the rings are the main force that pushes water through the nanocone. Comparing the flow rate of the vapor and liquid reservoirs, the vapor with the linear regime is more efficient as a harvesting mechanism.

Finally, we analyzed the impact in the flow of the presence of combined nanocones. In the case of two nanocones, we observed that for small distances $dr = 34$ Å, only one nanocone show a linear flow with time (FT regime), whereas the other collects only little droplets (SDCT regime). The interference is a consequence of the droplet formation at the base of one of the nanocones, whereas the other runs out of space for water condensation and capture. Increasing the distance $dr = 48$ Å, the competition decreases.

Consequently, when the number of nanocones is increased to four nanocones with a distance of $dr = 34$ Å between them, which means increasing the porosity, there is no temporal and spatial space to form a large droplet that leads to the FT regime. Then, the nanocones absorb small droplets over time remaining in the SDCT regime. Our results indicate that for having more efficient harvesting, all nanocones at FT regime, the distance between the nanocones have to be larger.

In conclusion, our study shows that water harvesting using hydrophilic sites is a potential way to capture water. We expect that this model can be employed in experiments.

ACKNOWLEDGMENTS

This work was supported by the Brazilian agencies CNPq (through INCT-Fcx) and CAPES (Coordenação de Aperfeiçoamento de Pessoal de Nível Superior). The authors are thankful for the computational infrastructure from CENAPAD/SP and CESUP/UFRGS.

AUTHOR DECLARATIONS

Conflict of Interest

The authors have no conflicts to disclose.

Author Contributions

Fernanda R. Leivas: Conceptualization (equal); Data curation (equal); Formal analysis (equal); Funding acquisition (equal); Investigation (equal); Methodology (equal); Project administration (equal); Software (equal); Validation (equal); Visualization (equal); Writing – original draft (equal). **Marcia C. Barbosa**: Conceptualization (equal); Formal analysis (equal); Investigation (equal); Methodology (equal); Project administration (equal); Supervision (equal); Validation (equal); Writing – original draft (equal).

DATA AVAILABILITY

The data that support the findings of this study are available from the corresponding author upon reasonable request.

REFERENCES

[1] M. F. Chaplin, Biochem. Mol. Biol. Educ. **29**, 54 (2001).
[2] M. M. Mekonnen and A. Y. Hoekstra, Sci. Adv. **2**, e1500323 (2016).
[3] A. M. Mapulanga and H. Naito, Proc. Natl. Acad. Sci. U. S. A. **116**, 8249 (2019).
[4] M. Milano, E. Reynard, G. Muniz-Miranda, and J. Guerrin, Water **10**, 1517 (2018).
[5] S. Desbureaux and A.-S. Rodella, World Dev. **114**, 13 (2019).
[6] D. Verner, *Reducing Poverty, Protecting Livelihoods, and Building Assets in a Changing Climate*, edited by D. Verner (The World Bank, 2010).
[7] H. Jarimi, R. Powell, and S. Riffat, Int. J. Low-Carbon Technol. **15**, 253 (2020).
[8] J. Y. Wang, J. Y. Liu, R. Z. Wang, and L. W. Wang, Appl. Therm. Eng. **127**, 1608 (2017).
[9] D. P. Ura, J. Knapczyk-Korczak, P. K. Szewczyk, E. A. Sroczyk, T. Busolo, M. M. Marzec, A. Bernasik, S. Kar-Narayan, and U. Stachewicz, ACS Nano **15**, 8848 (2021).
[10] A. LaPotin, H. Kim, S. R. Rao, and E. N. Wang, Acc. Chem. Res. **52**, 1588 (2019).
[11] L. Zhong, L. Zhu, J. Li, W. Pei, H. Chen, S. Wang, A. Razaa, A. Khan, Y. Hou, and Y. Zheng, Mol. Syst. Des. Eng. **6**, 986 (2021).
[12] P. S. Brown and B. Bhushan, Philos. Trans. R. Soc. A **374**, 135 (2016).
[13] L. Al-Ghussain, Environ. Prog. Sustainable Energy **38**, 13 (2019).
[14] Y. Tu, R. Wang, Y. Zhang, and J. Wang, Joule **2**, 1452 (2018).
[15] H. Bai, C. Zhang, Z. Long, H. Geng, T. Ba, Y. Fan, C. Yu, K. Li, M. Cao, and L. Jiang, J. Mater. Chem. A **6**, 20966 (2018).
[16] X. Dai, N. Sun, S. O. Nielsen, B. B. Stogin, J. Wang, S. Yang, and T.-S. Wong, Sci. Adv. **4**, eaaq0919 (2018).
[17] X. Wang, J. Zeng, X. Yu, C. Liang, and Y. Zhang, Appl. Surf. Sci. **465**, 986 (2019).
[18] M. Cao, J. Xiao, C. Yu, K. Li, and L. Jiang, Small **11**, 4379 (2015).
[19] M. De Marzio, G. Camisasca, M. M. Conde, M. Rovere, and P. Gallo, J. Chem. Phys. **146**, 084505 (2017).
[20] J. Engstler and N. Giovambattista, J. Chem. Phys. **157**, 064701 (2022).
[21] X. Qin, Q. Yuan, Y. Zhao, S. Xie, and Z. Liu, Nano Lett. **11**, 2173–2177 (2011).
[22] H. R. Corti, G. A. Appignanesi, M. C. Barbosa, J. R. Bordin, C. Calero, G. Camisasca, M. D. Elola, G. Franzese, P. Gallo, A. Hassanali, K. Huang, D. Laria, C. A. Menéndez, J. M. Montes de Oca, M. P. Longinotti, J. Rodriguez, M. Rovere, D. Scherlis, and I. Szleifer, Eur. Phys. J. E **44**, 136 (2021).
[23] J. K. Holt, H. G. Park, Y. Wang, M. Stadermann, A. B. Artyukhin, C. P. Grigoropoulos, A. Noy, and O. Bakajin, Science **312**, 1034 (2006).
[24] M. H. Köhler, J. R. Bordin, L. B. da Silva, and M. C. Barbosa, Physica A **490**, 331 (2018).
[25] J. R. Bordin and M. C. Barbosa, Physica A **467**, 137 (2017).
[26] J. Hassan, G. Diamantopoulos, D. Homouz, and G. Papavassiliou, Nanotechnol. Rev. **5**, 341 (2016).
[27] P. Sarapat, N. Thamwattana, B. J. Cox, and D. Baowan, J. Math. Chem. **58**, 1650–1662 (2020).
[28] W. Li, W. Wang, Y. Zhang, Y. Yan, P. Král, and J. Zhang, Carbon **129**, 374 (2018).
[29] M. Razmkhah, A. Ahmadpour, M. T. H. Mosavian, and F. Moosavi, Desalination **407**, 103 (2017).
[30] Z. Zhou, T. Gao, S. McCarthy, A. Kozbial, S. Tan, D. Pekker, L. Li, and P. W. Leu, Carbon **152**, 474 (2019).
[31] S. Ozden, L. Ge, T. N. Narayanan, A. H. C. Hart, H. Yang, S. Sridhar, R. Vajtai, and P. M. Ajayan, ACS Appl. Mater. Interfaces **6**, 10608 (2014).
[32] Y. Song, N. Xu, G. Liu, H. Qi, W. Zhao, B. Zhu, L. Zhou, and J. Zhu, Nat. Nanotechnol. **17**, 857 (2022).
[33] U. Legrand, D. Klassen, S. Watson, A. Aufoujal, B. Nisol, R. Boudreault, K. E. Waters, J.-L. Meunier, P.-L. Girard-Lauriault, M. R. Wertheimer, and J. R. Tavares, Ind. Eng. Chem. Res. **60**, 12923 (2021).
[34] A. Barati Farimani and N. R. Aluru, J. Phys. Chem. B **115**, 12145 (2011).
[35] M. H. Köhler, J. R. Bordin, C. F. de Matos, and M. C. Barbosa, Chem. Eng. Sci. **203**, 54 (2019).
[36] W. Li, W. Wang, X. Zheng, Z. Dong, Y. Yan, and J. Zhang, Comput. Mater. Sci. **136**, 60 (2017).

[37]M. Curcio, G. Cirillo, F. Saletta, F. Michniewicz, F. P. Nicoletta, O. Vittorio, S. Hampel, and F. Iemma, J. Carbon Res. **7**, 3 (2020).
[38]W. Li, Y. Yan, M. Wang, P. Král, C. Dai, and J. Zhang, J. Phys. Chem. Lett. **8**, 435–439 (2017).
[39]W. Li, W. Wang, Q. Hou, Y. Yan, C. Dai, and J. Zhang, Phys. Chem. Chem. Phys. **20**, 27910 (2018).
[40]F. R. Leivas and M. C. Barbosa, Beilstein J. Nanotechnol. **14**, 1 (2023).
[41]T. A. Schaub, Angew. Chem., Int. Ed. **59**, 4620 (2020).
[42]C. Pagura, S. Barison, C. Mortalò, N. Comisso, and M. Schiavon, Nanosci. Nanotechnol. Lett. **4**, 160 (2012).
[43]D. Voiry, G. Pagona, E. D. Canto, L. Ortolani, V. Morandi, L. Noé, M. Monthioux, N. Tagmatarchis, and A. Penicaud, Chem. Commun. **51**, 5017 (2015).
[44]N. Karousis, I. Suarez-Martinez, C. P. Ewels, and N. Tagmatarchis, Chem. Rev. **116**, 4850 (2016).
[45]S. Zhu and G. Xu, Nanoscale **2**, 2538 (2010).
[46]K. H. Jensen, A. X. C. N. Valente, and H. A. Stone, Phys. Fluids **26**, 052004 (2014).
[47]S. Mondal, I. M. Griffiths, and G. Z. Ramon, J. Membr. Sci. **588**, 117166 (2019).
[48]W. Huang, Z. Wang, F. Xie, H. Ding, W. Li, X. Liang, X. Ma, and Z. Xu, Desalination **538**, 115909 (2022).
[49]J. P. Kleinubing Abal and M. C. Barbosa, J. Chem. Phys. **154**, 134506 (2021).
[50]Y. Chen, Y. Li, Y. Li, J. Guo, S. Li, and S. Zhang, ACS Appl. Mater. Interfaces **13**, 59329 (2021).
[51]J. L. F. Abascal, E. Sanz, and C. Vega, Phys. Chem. Chem. Phys. **11**, 556 (2009).
[52]A. Chandra and P. Keblinski, J. Chem. Phys. **153**, 124505 (2020).
[53]A. Rokoni and Y. Sun, J. Chem. Phys. **153**, 144706 (2020).
[54]C. Vega, J. L. F. Abascal, and I. Nezbeda, J. Chem. Phys. **125**, 034503 (2006).
[55]I. N. Tsimpanogiannis, O. A. Moultos, L. F. Mercier Franco, M. B. de M. Spera, M. Erdos, and I. G. Economou, Mol. Simul. **45**, 425 (2018).
[56]C. Vega and E. de Miguel, J. Chem. Phys. **126**, 154707 (2007).
[57]J. Alejandre and G. A. Chapela, J. Chem. Phys. **132**, 014701 (2010).
[58]A. Krishnan, E. Dujardin, M. M. J. Treacy, J. Hugdahl, S. Lynum, and T. W. Ebbesen, Nature **388**, 451 (1997).
[59]J. L. F. Abascal and C. Vega, J. Chem. Phys. **123**, 234505 (2005).
[60]C. Vega and J. L. F. Abascal, Phys. Chem. Chem. Phys. **13**, 19663 (2011).
[61]V. Vinš, D. Celný, B. Planková, T. Němec, M. Duška, and J. Hrubý, EPJ Web Conf. **114**, 02136 (2016).
[62]J. Losey, S. K. Kannam, B. D. Todd, and R. J. Sadus, J. Chem. Phys. **150**, 194501 (2019).
[63]J. P. K. Abal and M. C. Barbosa, Phys. Chem. Chem. Phys. **23**, 12075 (2021).
[64]B. H. S. Mendonça, P. Ternes, E. Salcedo, A. B. de Oliveira, and M. C. Barbosa, J. Chem. Phys. **152**, 024708 (2020).
[65]J. R. Bordin, A. Diehl, M. C. Barbosa, and Y. Levin, Phys. Rev. E **85**, 031914 (2012).
[66]D. N. de Freitas, B. H. S. Mendonça, M. H. Köhler, M. C. Barbosa, M. J. S. Matos, R. J. C. Batista, and A. B. de Oliveira, Chem. Phys. **537**, 110849 (2020).